# Generation of Light with Multimode Time-Delayed Entanglement Using Storage in a Solid-State Spin-Wave Quantum Memory

Kate R. Ferguson,[1,*] Sarah E. Beavan,[2] Jevon J. Longdell,[3] and Matthew J. Sellars[1]
[1]Centre for Quantum Computation and Communication Technology, Laser Physics Centre, Australian National University, Canberra, Australian Capital Territory 2601, Australia
[2]European Space Agency, NL-2200 AG, Noordwijk, The Netherlands
[3]Jack Dodd Centre for Photonics and Ultra-Cold Atoms, Department of Physics, University of Otago, Dunedin 9016, New Zealand
(Received 7 February 2016; published 6 July 2016)

Here, we demonstrate generating and storing entanglement in a solid-state spin-wave quantum memory with on-demand readout using the process of rephased amplified spontaneous emission (RASE). Amplified spontaneous emission (ASE), resulting from an inverted ensemble of $Pr^{3+}$ ions doped into a $Y_2SiO_5$ crystal, generates entanglement between collective states of the praseodymium ensemble and the output light. The ensemble is then rephased using a four-level photon echo technique. Entanglement between the ASE and its echo is confirmed and the inseparability violation preserved when the RASE is stored as a spin wave for up to 5 $\mu$s. RASE is shown to be temporally multimode with almost perfect distinguishability between two temporal modes demonstrated. These results pave the way for the use of multimode solid-state quantum memories in scalable quantum networks.

DOI: 10.1103/PhysRevLett.117.020501

Photonic quantum memories are essential devices in quantum information science. The role of a quantum memory, which can store and retrieve information encoded on photons, is to enable the synchronization of probabilistic quantum processes, e.g., in quantum communication [1] and computing [2]. Storing the information carried by photons requires strong interactions between single photons and matter. While sufficiently strong interactions can be obtained by placing individual quantum systems in high finesse cavities [3], atomic ensembles provide an attractive alternative.

Rare-earth ion-doped crystals (REICs) are particularly promising due to long coherence times on both the optical and hyperfine transitions [4] while being free from decoherence due to atomic motion and offering a platform for integration [5]. Currently, the low bandwidth of REIC memories makes it difficult to interface them with spontaneous parametric down conversation sources. Many demonstrations have shown storage of entangled [6,7] and heralded single photons [8]. However, these nonclassical states were stored in memories with fixed storage times, and the ability to read stored states out on-demand is essential for the synchronizing functionality of a quantum memory. The difficulty of interfacing entangled pair sources and REIC quantum memories means that on-demand solid-state quantum memory demonstrations have stored weak coherent states [9–11].

The difficulty with interfacing sources also limits atomic gas quantum memories; however, a solution was proposed by Duan, Lukin, Cirac, and Zoller (DLCZ). In the DLCZ protocol, nonclassical states are generated from atomic ensembles using Raman transitions that lead to nonclassical correlations between atomic excitations and emitted photons [12]. The collective atomic excitations, called spin waves, can be efficiently readout in a well-defined spatial mode due to constructive interference of the atoms involved. To date, no quantum solid-state DLCZ implementation has been demonstrated [13].

Recently, the rephased amplified spontaneous emission scheme (RASE) was proposed, which has strong parallels to DLCZ, generating a collective atomic state via the measurement of spontaneous emission and rephasing of it using photon echo techniques [14]. Using resonant photon echo techniques has the advantage that the bright driving fields are off when the signals are being detected, as opposed to the nonresonant Raman techniques used in DLCZ, increasing the possibility of low noise operation. Long optical coherence times, which are present in REICs but not in atomic gas systems, are required to implement this technique. Spin-wave storage is inherent in the four-level version of RASE (4L-RASE) [15]. The advantage of the RASE and DLCZ schemes is that nonclassical states are both generated and stored in the same protocol, so the entangled light is automatically the correct wavelength and bandwidth. This will greatly improve the ease of integration.

In the basic RASE scheme, the population of an inhomogeneously broadened ensemble of "two-level" atoms is inverted. The gain of the ensemble then amplifies the input vacuum fluctuations, emitting amplified spontaneous emission (ASE). While ASE on its own is considered a noisy field, this noise is due to entanglement generated between it and the collective modes of the amplifying medium. The ensemble inhomogeneity ensures that the collective atomic state dephases; however, for systems such

 

as REICs with long coherence times, these internal degrees of freedom can be rephased in a manner analogous to a photon echo [16]. The RASE scheme allows for the state of the amplifying medium to be readout as a second optical field, the RASE, which is entangled with the ASE.

Experimental investigations of RASE have been previously investigated using both two levels [17] and four levels [15]. The four-level work used storage in a spin wave but was only able to show classical correlations due to the challenging spectral filtering requirements associated with discrete-variable detection. The two level RASE experiment came closer to showing entanglement but didn't incorporate spin-wave storage. Here, for the first time, we show entanglement between the time-separated ASE and RASE fields after storage of the RASE field as a spin wave. Continuous-variable detection is used to spectrally discriminate emission to nearby hyperfine levels.

The 4L-RASE pulse sequence is depicted in the frequency and temporal domain in Figs. 1(b) and 1(c), respectively. The four-level sequence rephases coherence generated between two levels (here, $|2\rangle \leftrightarrow |4\rangle$) while transferring it to two completely different levels ($|3\rangle \leftrightarrow |5\rangle$). This is achieved by applying two sequential rephasing $\pi$ pulses driving transitions $|3\rangle \leftrightarrow |4\rangle$ and $|2\rangle \leftrightarrow |5\rangle$. The free-induction decay resulting from the two $\pi$ pulses is now spectrally resolvable from both the ASE and RASE emission. Following the application of the first $\pi$ pulse the entangled state is stored on the long-lived hyperfine ground states as a spin wave before being transferred back to the optical transition by the second $\pi$ pulse.

The sample used in this experiment was a $2 \times 4 \times 5$ mm 0.005% $Pr^{3+}:Y_2SiO_5$ (Pr:YSO) crystal cooled to 4.2 K using exchange gas cooling in a liquid helium bucket cryostat. There is only vertical optical access to the cryostat, so a back mirror reflects the light back through the sample to an optics platform on top of the cryostat. The experimental arrangement is shown in Fig. 1(a). The energy level structure of Pr:YSO is depicted in Fig. 1(b). The lifetime for the excited state is $T_1 = 164$ $\mu$s [18] and the dephasing time was measured here to be $T_2^*$ 151 $\mu$s. The lifetime between the ground state hyperfine levels is ~200 s [19] and the coherence time is ~500 $\mu$s at zero magnetic field [20], so potentially long storage times are obtainable. All the optical transitions are weakly allowed with the transition strengths reported in Ref. [21].

The optical decay time for the four-level sequence used for the RASE scheme was measured to be 53 $\mu$s. This is roughly a third of the coherence time for the standard two-level echo. The discrepancy is attributed to a component of inhomogeneity on the spin levels that is not rephased using the four-level sequence [22].

The optical $^3H_4 \rightarrow {}^1D_2$ transition is inhomogeneously broadened to 3 GHz, 2 orders of magnitude larger than the ~10 MHz hyperfine splittings. Before each shot of the RASE experiment, a subgroup of ions with 150 kHz inhomogeneity is selected and the population initialized into $|1\rangle$ using spectral hole-burning techniques similar to those described in Refs. [15,21].

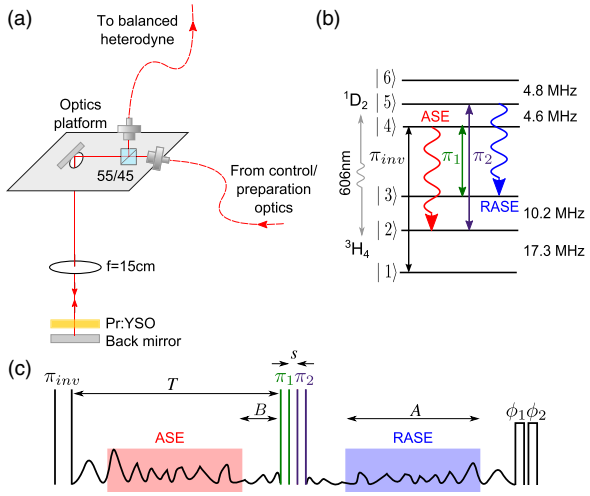


FIG. 1. (a) RASE setup. The 0.005% Pr:YSO crystal, lens, and back mirror are located at the bottom of a liquid helium bucket cryostat at 4.2 K. The cryostat only has vertical optical access, so a top optics platform has fibre couplers steering the control and preparation beams into the cryostat and the reflected signal beam to the balanced heterodyne detection system. (b) Hyperfine levels of the ground $^3H_4$ and excited $^1D_2$ manifold in Pr:YSO. For the RASE experiment, a subensemble of ions is selected using spectral hole burning and prepared to be initially in state $|1\rangle$. The frequencies used to apply the 4L-RASE protocol are marked. (c) Pulse sequence used in a single shot of the 4L-RASE experiment. After the inversion pulse $\pi_{\text{inv}}$ is applied, the ensemble is allowed to spontaneously emit for $T$ before the rephasing pulses $\pi_1 = 1.5$ $\mu$s and $\pi_2 = 2.2$ $\mu$s are applied. These are separated by a time $s$, the storage time on the spin states. $A$ is the length of the ASE and RASE windows used for calculating the quadrature values. $B$ is the delay between the end (start) of the ASE (RASE) window and the rephasing pulses to allow the detectors to recover from saturation due to the intense $\pi$ pulses. After the sequence, two weak phase reference pulses, $\phi_1$ and $\phi_2$, are applied to correct for the frequency dependent phase offsets shot to shot.

After selecting out the ensemble, a single shot of the RASE experiment is performed. The ensemble preparation takes ~100 ms limiting the repetition rate of the experiment to 10 Hz. The temporal sequence is outlined in Fig. 1(c). For the first experiment $s = 0$ $\mu$s, $T = 18.5$ $\mu$s, $A = 10$ $\mu$s, and $B = 5$ $\mu$s. The inversion pulse creates a gain feature with optical depth of $\alpha l = 2.35$ [23]. The control beam is gated on with a double-pass acousto-optic modulator. Shot noise limited heterodyne detection is used to characterize the ASE and RASE fields by measuring the variances of the amplitude $\hat{x}$ and phase $\hat{p}$ quadratures of light. The phase of the interferometer was not locked and was different shot to shot. The phase between the different frequency rf pulses was not constant either. Two phase reference pulses applied after the 4L-RASE sequence allowed the data to be corrected for these two issues [23].

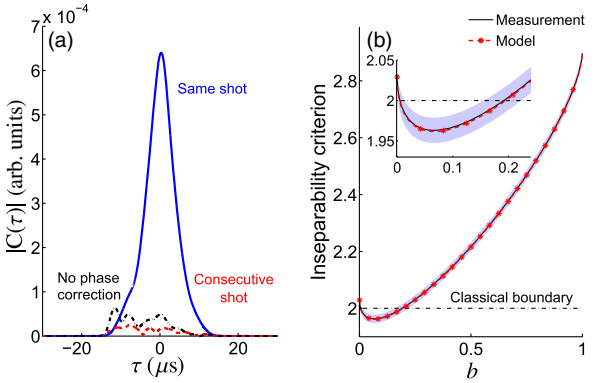


FIG. 2. (a) The cross-correlation function between the ASE and RASE fields [Eq. (1)] of the same shot, consecutive shots, and when the phase correction is not applied averaged over 8000 trials. (b) The inseparability criterion [Eq. (3)] as a function of $b$ when $s = 0$. The ASE (RASE) variance is $1.453 \pm 0.023$ ($1.015 \pm 0.016$) normalized to the vacuum. The shaded area indicates $1\sigma$ confidence. Inset shows a close up of the minimum of the inseparability criterion.

The first way of characterizing the correlation between the ASE and RASE fields is by evaluating the cross-correlation of the two fields. The rephasing sequence ideally results in a time-reversed, conjugated version of the ASE field so the cross-correlation is defined as

$$C(\tau) = \int A(t)R(\tau - t)dt, \tag{1}$$

where $A(t)$ [$R(t)$] is the amplitude of the ASE (RASE) field and $\tau = 0$ has been chosen to correspond to the center of the two rephasing pulses. The integral is over all time and $A(t)$ and $R(t)$ are windowed such that they are zero outside the time windows shown in Fig. 1(c).

Figure 2(a) shows the mean cross-correlation between the ASE and RASE of the same shots, of different shots, and when the phase correction is not applied. There is a distinct correlation peak only present when comparing the ASE and RASE of the same shot, so there is no evidence of correlations due to coherent effects. This confirms a time-separated correlation between the ASE and RASE fields. The 7 $\mu$s temporal width of the correlation peak corresponds to a 65 kHz ASE bandwidth.

To test the quantum nature of this time-separated correlation, the inseparability criterion for continuous variable states created by Duan *et al.* is used [24]. A maximally entangled state can be expressed as a coeigenstate of a pair of EPR-type operators

$$\hat{u} = \sqrt{b}\hat{x}_1 + \sqrt{1-b}\hat{x}_2, \quad \hat{v} = \sqrt{b}\hat{p}_1 - \sqrt{1-b}\hat{p}_2, \tag{2}$$

where $b \in [0, 1]$ is a weighting parameter describing the weight given to the ASE and RASE fields. The subscript 1(2) indicates the ASE (RASE) field.

For any separable state, the total variance of $\hat{u}$ and $\hat{v}$ satisfies

$$\langle(\Delta\hat{u})^2\rangle + \langle(\Delta\hat{v})^2\rangle \geq 2. \tag{3}$$

For inseparable states, the total variance is bound from below by zero.

Heterodyne detection provides simultaneous, noisy measurements of both the light quadratures [25] as opposed to homodyne detection which provides a good measure of just one quadrature. The same inseparability criterion can be used for both detection methods; however, the size of the correlation will be reduced by a factor of 2 when using a heterodyne detector [17].

The complex valued heterodyne signal was windowed with a 10 $\mu$s temporal function that is a convolution of a top hat and a Gaussian function and then integrated to obtain values of $\hat{x}$ and $\hat{p}$ for both the ASE and RASE time windows. The spectral width of this window was optimized to match the spectral profile of the signals, giving the strongest correlation [23].

When $b = 1(0)$ the variance only consists of the ASE (RASE) field summed over both quadratures. The uncorrelated case is a straight line between these two values. Figure 2(b) shows the inseparability criterion verses $b$. There is a clear dip indicating a correlation between the ASE and RASE fields. At the lowest point, $\langle(\Delta\hat{u})^2\rangle + \langle(\Delta\hat{v})^2\rangle = 1.964$ at $b = 0.068$ violating the inseparability criterion with 98.6% confidence, a $2.2\sigma$ violation. The error in the variance was calculated as in [17]. The low value of $b$ is due to the difference in size of the ASE and RASE fields due to the low rephasing efficiency of 3.2%, determined by the ratio of the signal variances.

Expected values for the inseparability criterion are calculated based on a simple model using the ASE variance and rephasing efficiency. The model assumes the ASE and RASE fields are initially maximally entangled, and this entanglement is then degraded by loss. The loss, due to the two beam splitters, reflection, and the detector efficiencies, is modeled as a single beam splitter in both the ASE and RASE modes, and the rephasing efficiency is modeled as an additional beam splitter in the RASE mode [23]. The measured inseparability tracks almost perfectly with the modeled criterion indicating very little noise is added during the rephasing process.

The limitation in this experiment is the rephasing efficiency, which should increase with increasing optical depth (OD) [17,26]; however, it was seen to saturate at ~3%. Perfect rephasing $\pi$ pulses were not possible in the present configuration, where the control fields and signals were in the same mode, and the optically thick sample distorted the pulses to a larger degree as the OD increased. The distortion introduced additional noise such that the measured inseparability criterion no longer agreed with the model for large OD. The efficiency can theoretically approach 100% by placing the sample in a low finesse

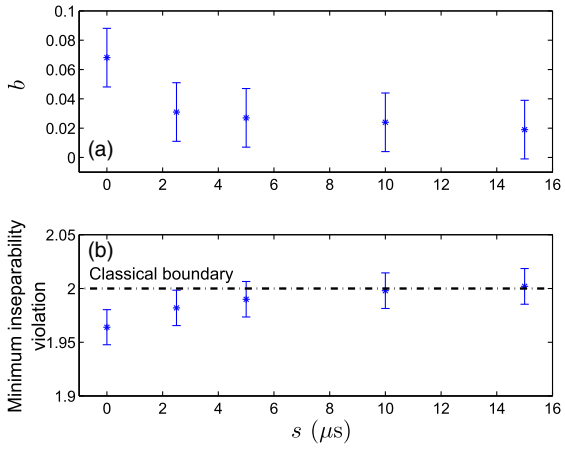


FIG. 3. (a) $b$ and (b) the minimum inseparability violation with increasing spin-wave storage time $s$. All error bars are $1\sigma$.

cavity [27]. In this case, the trade off between rephasing pulse uniformity and optical depth could be avoided by applying the $\pi$ pulses off axis. Efficiency enhancement has similarly been shown for DLCZ by placing cold atoms in a ring cavity [28].

Next, we investigated the spin-wave storage of the quantum memory by varying $s$. The total storage time is $T_s = 2B + s$. The dephasing caused by the inhomogeneous broadening on the spin states is not rephased by the four-level sequence resulting in a decay of $b$ with increasing $s$ [Fig. 3(a)] as the rephasing efficiency drops. In Fig. 3(b), the minimum inseparability violation gets correspondingly worse until the criterion is at the classical boundary for $s = 10$ $\mu$s and $s = 15$ $\mu$s ($T_s = 20$–$25$ $\mu$s). It should be possible to increase the storage time by applying rephasing rf $\pi$ pulses to the hyperfine levels [4,29].

RASE is based on photon echo rephasing techniques, and, as such, should be inherently temporally multimode. In quantum repeater applications, the addition of multimode memories able to store and retrieve $N$ different modes while preserving their distinguishability can increase the overall success rate of the repeater by that factor $N$ [30].

To test the multimode capability of RASE, the signal windows in Fig. 1(c) are increased to $A = 20$ $\mu$s allowing two 10 $\mu$s temporal windows per shot. The labeling of the two temporal windows is shown in Fig. 4(a). The inseparability criteria for the four possible combinations of windows are shown in Fig. 4(b). The two combinations where the ASE and RASE windows are time symmetric around the rephasing pulses have a correlation between the two fields while the nonsymmetric combinations are almost completely uncorrelated, evidenced by the straight line criterion. The distinguishability between the different temporal modes is, therefore, almost perfectly preserved.

The two correlated temporal modes violate the inseparability criterion with 86% and 89% confidence for $A1R1$ and $A2R2$, respectively. $b$ is $\sim 3.5x$ smaller for $A1R1$

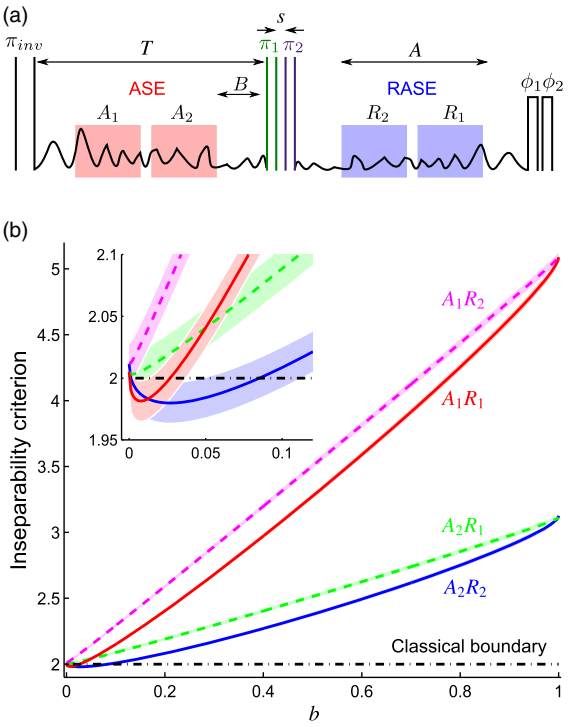


FIG. 4. (a) Pulse sequence used for the multimode 4L-RASE experiment showing the labeling of the two temporal modes. $A = 20$ $\mu$s, $B = 5$ $\mu$s, $T = 28.5$ $\mu$s, and $s = 0$ $\mu$s. (b) Inseparability criterion for the four combinations of the two temporal modes. The solid lines are the time-symmetric combinations showing a correlation. The dashed lines are the nonsymmetric cases and are uncorrelated. The shaded areas indicate $1\sigma$ confidence. Inset shows a close up of the minimum of the criterion.

corresponding to a reduced rephasing efficiency further from the $\pi$ pulses.

In conclusion, we have demonstrated a means of generating entanglement and storing it on the spin states of a Pr:YSO crystal through rephasing spontaneous emission. We confirmed the temporal multimode capability of RASE inherent in the rephasing process. Combining temporal multiplexing and storage on the spin states allows the possibility of a simultaneous readout of different temporal modes from neighboring memories to perform entanglement swapping operations. While the current demonstration used continuous-variable detection, this scheme is equally capable of generating on-demand single photons. RASE takes advantage of the unique coherence properties of REICs to generate and store entangled states in a single protocol, paving the way to making scalable, solid-state quantum information processing architectures.

This work was supported by the Australian Research Council Centre of Excellence for Quantum Computation and Communication Technology (Grant No. CE110001027). M. J. S. was supported by an Australian Research Council Future Fellowship (Grant No. FT110100919). J. J. L. would like to acknowledge the Marsden Fund

(Contract No. UOO1520) of the Royal Society of New Zealand. The authors would like to acknowledge the support of the Australian Defense Science and Technology Group.

*Corresponding author.
katherine.ferguson@anu.edu.au

[1] N. Sangouard, C. Simon, H. de Riedmatten, and N. Gisin, Rev. Mod. Phys. **83**, 33 (2011).
[2] E. Knill, R. Laflamme, and G. J. Milburn, Nature (London) **409**, 46 (2001).
[3] H. P. Specht, C. Nölleke, A. Reiserer, M. Uphoff, E. Figueroa, S. Ritter, and G. Rempe, Nature (London) **473**, 190 (2011).
[4] M. Zhong, M. P. Hedges, R. L. Ahlefeldt, J. G. Bartholomew, S. E. Beavan, S. M. Wittig, J. J. Longdell, and M. J. Sellars, Nature (London) **517**, 177 (2015).
[5] S. Marzban, J. G. Bartholomew, S. Madden, K. Vu, and M. J. Sellars, Phys. Rev. Lett. **115**, 013601 (2015).
[6] C. Clausen, I. Usmani, F. Bussieres, N. Sangouard, M. Afzelius, H. de Riedmatten, and N. Gisin, Nature (London) **469**, 508 (2011).
[7] E. Saglamyurek, N. Sinclair, J. Jin, J. A. Slater, D. Oblak, F. Bussières, M. George, R. Ricken, W. Sohler, and W. Tittel, Nature (London) **469**, 512 (2011).
[8] D. Rieländer, K. Kutluer, P. M. Ledingham, M. Gündoğan, J. Fekete, M. Mazzera, and H. de Riedmatten, Phys. Rev. Lett. **112**, 040504 (2014).
[9] M. P. Hedges, J. J. Longdell, Y. Li, and M. J. Sellars, Nature (London) **465**, 1052 (2010).
[10] M. Gündoğan, P. M. Ledingham, K. Kutluer, M. Mazzera, and H. de Riedmatten, Phys. Rev. Lett. **114**, 230501 (2015).
[11] C. Laplane, P. Jobez, J. Etesse, N. Timoney, N. Gisin, and M. Afzelius, New J. Phys. **18**, 013006 (2016).
[12] L. M. Duan, M. D. Lukin, J. I. Cirac, and P. Zoller, Nature (London) **414**, 413 (2001).
[13] E. A. Goldschmidt, S. E. Beavan, S. V. Polyakov, A. L. Migdall, and M. J. Sellars, Opt. Express **21**, 10087 (2013).
[14] P. M. Ledingham, W. R. Naylor, J. J. Longdell, S. E. Beavan, and M. J. Sellars, Phys. Rev. A **81**, 012301 (2010).
[15] S. E. Beavan, M. P. Hedges, and M. J. Sellars, Phys. Rev. Lett. **109**, 093603 (2012).
[16] N. A. Kurnit, I. D. Abella, and S. R. Hartmann, Phys. Rev. Lett. **13**, 567 (1964).
[17] P. M. Ledingham, W. R. Naylor, and J. J. Longdell, Phys. Rev. Lett. **109**, 093602 (2012).
[18] R. W. Equall, R. L. Cone, and R. M. Macfarlane, Phys. Rev. B **52**, 3963 (1995).
[19] K. Holliday, M. Croci, E. Vauthey, and U. P. Wild, Phys. Rev. B **47**, 14741 (1993).
[20] E. Fraval, Ph.D. thesis, Australian National University, 2006.
[21] M. Nilsson, L. Rippe, S. Kröll, R. Klieber, and D. Suter, Phys. Rev. B **70**, 214116 (2004).
[22] S. E. Beavan, P. M. Ledingham, J. J. Longdell, and M. J. Sellars, Opt. Lett. **36**, 1272 (2011).
[23] See Supplemental Material at http://link.aps.org/supplemental/10.1103/PhysRevLett.117.020501 for details of gain measurements, the windowing of the ASE and RASE signals, and the inseparability criterion model.
[24] L.-M. Duan, G. Giedke, J. I. Cirac, and P. Zoller, Phys. Rev. Lett. **84**, 2722 (2000).
[25] H. P. Yuen and V. W. S. Chan, Opt. Lett. **8**, 177 (1983).
[26] R. N. Stevenson, M. R. Hush, A. R. R. Carvalho, S. E. Beavan, M. J. Sellars, and J. J. Hope, New J. Phys. **16**, 033042 (2014).
[27] L. A. Williamson and J. J. Longdell, New J. Phys. **16**, 073046 (2014).
[28] X.-H. Bao, A. Reingruber, P. Dietrich, J. Rui, A. Dück, T. Strassel, L. Li, N.-L. Liu, B. Zhao, and J.-W. Pan, Nat. Phys. **8**, 517 (2012).
[29] E. Fraval, M. J. Sellars, and J. J. Longdell, Phys. Rev. Lett. **92**, 077601 (2004).
[30] C. Simon, H. de Riedmatten, M. Afzelius, N. Sangouard, H. Zbinden, and N. Gisin, Phys. Rev. Lett. **98**, 190503 (2007).